Single-layer narrow-band beam splitter based on a transparent grating with high-spectral contrast and high-angle sensitivity

Jian Zhang, Xinping Zhang ✉

Institute of Information Photonics Technology and College of Applied Sciences, Beijing University of Technology, Beijing 100124, People's Republic of China
✉ *E-mail: zhangxinping@bjut.edu.cn*

Published in Micro & Nano Letters; Received on 20th February 2017; Revised on 18th April 2017; Accepted on 7th June 2017

A report on the polarisation beam splitter with high-angle-resolved tunability in the visible spectrum, which was achieved in a single layer of transparent thin film of indium-tin-oxide (ITO). One-dimensional grating structures were etched into an ITO layer with a designed depth using inductively coupled plasma, where the remaining ITO acts as a waveguide. Enhanced reflection of light was observed when the retro-diffraction was overlapped with the waveguide resonance mode. A beam splitting ratio of 1:1 was achieved at 532 nm at a specific incident angle. This is a stable and efficient beam splitter with high contrast and narrow-band response. It can also be applied as tunable narrow-band filters, angle sensors or optical switch.

1. Introduction: Photonic devices combining periodic structures and waveguides show flexibly tunable resonance modes with high-spectral selectivity, which have a variety of 'derivatives' with multi-fold tunability through changing the structural parameters [1–3]. Changing the shape of the grating structures provides another dimension in tuning the optical response, where rectangular [4], triangular [5], and sinusoidal [6] gratings have been demonstrated for different purposes. Such structures have been applied extensively in optical filters [7, 8], optical polarisers [9, 10], plasmonic sensors [11, 12], optical switches [13], beam splitters [14, 15], and distributed feedback (DFB) lasers [16, 17]. Waveguide grating structures have been studied extensively both experimentally and theoretically [3, 18] with a variety of applications explored in optical engineering [19] and in sensors [11, 12, 20]. We note that the waveguide resonance modes in such structures may overlap other diffraction- or waveguide-related processes to enhance their optical response in intensity and in sensitivity. For instance, diffraction anomaly and Bragg diffraction may coexist with the waveguide resonance mode [16, 21]. Such overlapping or coupling effects may not only strengthen specific photophysical functions; however, also extending applications of such devices. In this research, we observed a retro-diffraction process that is overlapped with the waveguide resonance mode within a selected spectrum, which is equivalent to a second-order Bragg diffraction. Efficient optical beam-splitting and filtering effects with narrow-band resonance and high spectral contrast has been achieved. Although waveguide grating structures have been investigated extensively [1–3, 22–25], the overlap between these two different resonance modes to produce a more efficient optical modulation has not been observed and investigated in such structures. The corresponding device was produced by etching a nanoscale grating into a transparent waveguide layer of indium-tin-oxide (ITO). The high-surface quality and high-waveguide- and grating-homogeneity ensured high efficiency and high contrast in the spectroscopic response. These excellent performances have rarely been demonstrated for such transparent grating structures.

2. Design and fabrication of the thin-film grating: Commercial ITO glass substrates were employed for preparing the beam-splitting device, where the ITO layer has a thickness of about 200 nm. The ITO film has stable physical and chemical properties, which has very low absorption in visible spectrum. These features make ITO a suitable candidate for applications in practical optical devices. Furthermore, the ITO glass substrates have high surface quality, homogeneous film thickness, and low cost as a commercial material. Interference lithography using S1805 photoresist and subsequent inductively coupled plasma (ICP) etching were employed to transfer the PR grating into the ITO layers. The fabrication procedures are illustrated schematically in Figs. 1*a*–*d*. The positive photoresist S1805 was spin-coated at a speed of 2000 rpm onto a piece of ITO glass substrate with an area of 15×15 mm^2 and a thickness of 1 mm. A 325-nm He-Cd laser from Kimmon was used as the UV light source for interference lithography. The period of the PR grating was adjusted by changing the angle (θ) between the interference beams using $\Lambda = \lambda/[2\sin(\theta/2)]$, where λ is the wavelength of the UV laser and θ is the separation angle between the two laser beams. Fig. 1*b* shows the fabricated PR mask grating after the exposure and development processes. Then, ICP etching was used to transfer the mask grating into the ITO layer. The ratio between the etching speeds for PR and for ITO is ~4:1. The PR mask should be high enough in order that we fabricate the ITO grating structures with desired modulation depth. Finally, ITO gratings with steep sidewalls were obtained after the remaining PR was removed by immersing the sample in acetone, as shown in Fig. 1*d*. Through adjusting the modulation depth of PR mask grating and the etching time, we can control the duty cycle and modulation depth of the ITO grating.

Figs. 1*e* and *f* show the scanning electron microscopic (SEM) and atomic force microscopic (AFM) images of the fabricated structures, respectively. The period of the grating is $\Lambda = 500$ nm and the duty cycle (w/Λ) is ~50%. The modulation depth of the grating is ~65 nm in Fig. 1, corresponding to a waveguide thickness of ~135 nm. An etching time of 60 s was employed for the structures in Figs. 1*e* and *f*, corresponding to an ITO-etching speed of ~1 nm/s.

It needs to be noted that the structural parameters in Fig. 1 have been optimised through a series of test experiments. A number of gratings have been produced with different duty cycles, different modulation depth, and different thickness of the ITO layer. Furthermore, ITO glass plates from different manufacturers have been tried for the fabrication. The grating period of 500 nm has been chosen in the consideration that a relatively large grating period may ease the etching process and produce grating lines with rectangular shapes, the resonance mode should be located in visible and in the transparent band of ITO, the tuning range of the resonance mode should cover the visible band from the blue

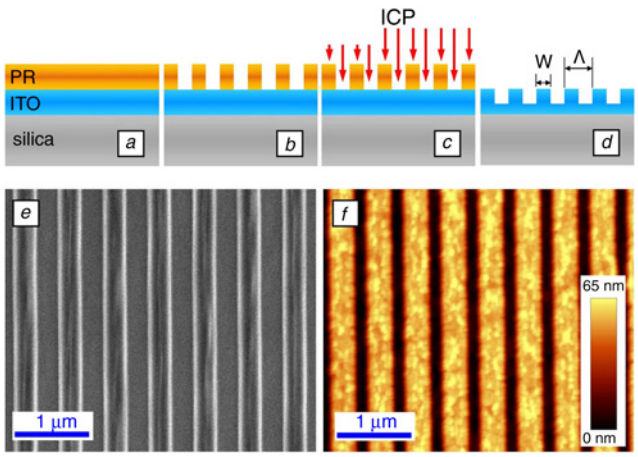

Fig. 1 *Schematic illustration for the fabrication of the ITO grating*
a Spin-coating of 400-nm PR film onto the ITO glass substrate
b Interference lithography for the fabrication of the PR grating
c ICP etching for transferring the PR grating into the ITO layer
d ITO grating after removal of the residual PR
e, *f* SEM and AFM images of the fabricated structures

to the red. The parameters shown in Fig. 1 satisfies the above conditions excellently.

3. Retro-diffraction enhanced resonance in a waveguide grating: Fig. 2 demonstrates the basic principles for the retro-diffraction-enhanced resonance mode of a waveguide grating, which only includes the reflection process at θ_r, the refraction process at θ_b, and the diffraction processes. The incident light at θ_i is first diffracted by the ITO grating into the ITO waveguide at θ_d through $a+1$-order process:

$$\Lambda(\sin\theta_i + n_{\mathrm{ITO}} \cdot \sin\theta_d) = \lambda. \tag{1}$$

where Λ is the grating period, n_{ITO} is the refractive index of ITO, and λ is the wavelength of light. This process is illustrated by the 'red' to 'white' arrows in Fig. 2

The diffracted light beam is then totally reflected by the ITO/substrate interface and reaches the top grating from the bottom side. A subsequent second-order diffraction enables a retro-reflection-like process, as indicated by the 'white' and 'yellow' arrows, which can be written as:

$$2\Lambda \cdot n_{\mathrm{ITO}} \times \sin\theta_d = 2\lambda. \tag{2}$$

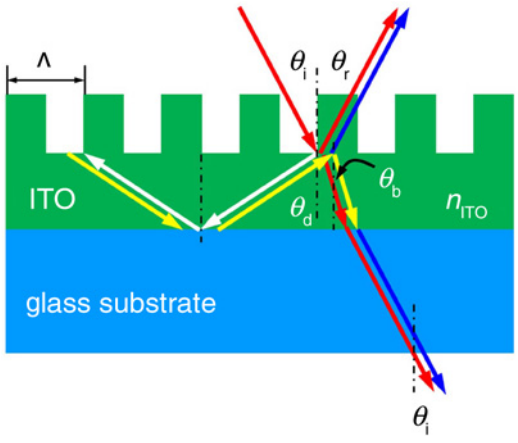

Fig. 2 *Retro-diffraction enhanced resonance modes in a waveguide-grating splitter*

Subtracting (1) from (2), we obtain:

$$\Lambda(n_{\mathrm{ITO}} \cdot \sin\theta_d - \sin\theta_i) = \lambda. \tag{3}$$

Since $\theta_i = \theta_r$, we actually have:

$$\Lambda(n_{\mathrm{ITO}} \cdot \sin\theta_d - \sin\theta_r) = \lambda. \tag{4}$$

which is equivalent to a diffraction from the waveguide into the reflection beam. Similar processes can also be understood in the transmission beam

$$n_{\mathrm{ITO}} \cdot \Lambda(\sin\theta_d - \sin\theta_b) = \lambda. \tag{5}$$

where θ_b equals the refraction angle and $\theta_i = \theta_r = \sin^{-1}(n_{\mathrm{ITO}} \cdot \sin\theta_b)$, as illustrated by the blue arrows in Fig. 2.

Actually, (4) and (5) define order diffraction processes of the incident light beam. However, the difference between the processes in Fig. 2 and a normal -1-order diffraction is that the conditions for retro-diffraction processes are satisfied at specified wavelengths and the corresponding incident angles, so that the resonance modes are enhanced significantly in the processes in Fig. 2. The diffracted beams interfere with the reflected and transmitted beams constructively and destructively, respectively, leading to enhanced reflection and reduced transmission processes. Above mechanisms will be observed as strong enhancement in a specific band in the transmission optical extinction spectrum. Furthermore, the condition for retro-reflection in (2) can also be taken as a second-order Bragg-like diffraction. This will be verified both by the spectroscopic performance in Section 4 and by the diffraction patterns in Section 5.

4. Spectroscopic performance: Figs. 3*a–d* show spectroscopic characterisation for understanding the enhanced resonance mode of the waveguide grating splitter. Figs. 3*a* and *c* show a 3D plot of the measurement results on transmission optical extinction as a function of wavelength and the angle of incidence for TE and TM polarisations, respectively, for a spectral range from 400 to 850 nm and an angle-resolve tuning range from 0 to ~48°. The optical extinction was calculated by $-\log_{10}(I/I_0)$, where I and I_0 are the transmission spectra through the grating and through the substrate, respectively. Thus, the values of optical extinction are in the units of optical density (OD). The retro-diffraction enhanced resonance modes can be observed in a spectral range from lesser than 500 nm to about 650 nm and in an incident angle range from ~15 to 45° for both TE and TM polarisation, corresponding to the efficient operation range of the devices, as marked by extended white braces. The resonance mode shifts to the blue with increasing the incident angle, agreeing well with the -1-order diffraction processes formulated by (3)–(5).

Figs. 3*b* and *d* show the optical extinction spectra within the efficient operation range ($\theta_i = 14$–$44°$, $\lambda = 450$–650 nm) of the device for TE and TM polarisations, respectively. For TE polarisation, the peak amplitude of the narrow-band optical extinction spectrum for the resonance mode is located at ~530 nm, which is as large as 0.34 OD, corresponding to a reduction of ~55% in the transmission spectrum. However, the TM-polarisation resonance mode becomes less efficient than the TE, where the peak amplitude of the optical extinction is also located at ~530 nm and it was reduced to ~0.22, corresponding to 40% reduction in the transmission spectrum. Fig. 3 also shows that the resonance modes have a bandwidth as narrow as 7 nm at full width at half maximum FWHM in most of the measured resonance spectra. We need to note that the transmission optical extinction or the reduction in the optical transmission implies redistribution of the incident light energy from transmission to the reflection. Meanwhile, the optical extinction spectra in Fig. 3 exhibit high contrast and symmetric line shapes. Therefore, the spectroscopic performance in Fig. 3 implies possible development of high-efficiency, high-contrast, and high-sensitivity beam splitting devices.

doi: 10.1049/mnl.2017.0082

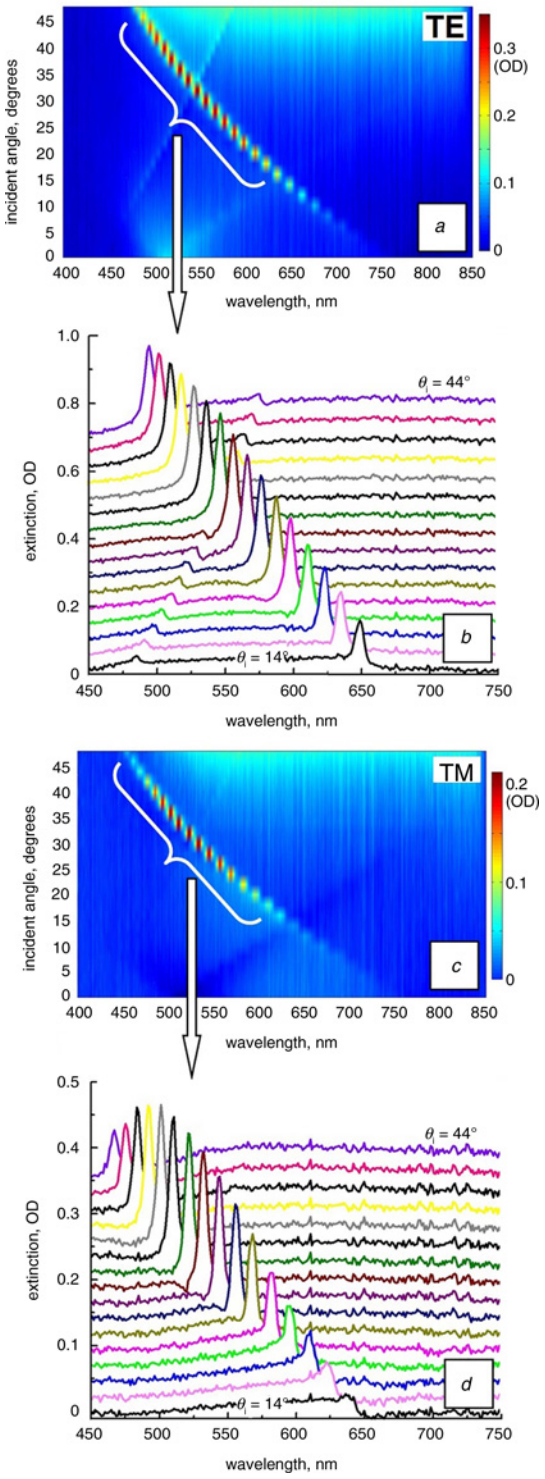

Fig. 3 *Optical extinction spectroscopic response of the waveguide grating splitter*
a, *c* 3D plots of optical extinction as a function of wavelength (400–850 nm) and angle of incidence (0–48°) for TE and TM polarisations, respectively
b, *d* Optical extinction spectra in a selected angle-resolved tuning range, as marked in Figs. 3*a* and *c*, for TE and TM polarisations, respectively

Furthermore, according to Figs. 3*a–d*, it is hard to observe the +1 order diffractions of the waveguide resonance mode. This not only verifies that the retro-diffraction overlaps only the −1 orders of diffractions, as modelled by (3), (4) or (5), but also confirms the strong enhancement of the resonance modes by the Bragg-like retro-diffraction processes. Based on above investigations, we studied the monochromatic beam splitting functions of such a waveguide grating in Section 4.

5. Beam splitting through retro-diffraction enhancement

5.1. Green-laser beam splitting at 532 nm: According to Fig. 3, the most efficient operation of the resonance mode of the waveguide-grating splitter device is located at ∼530 nm for both TE and TM polarisation. Therefore, we measured the beam splitting performance on the device using a green laser beam at 532 nm, as shown in Fig. 4, where photographs of the reflected laser spot were taken at a series of angles of incidence. Figs. 4*a–e* show the measurement results for TE polarisation and Figs. 4*f–j* for TM polarisation, where the incident angle was increased from 24 to 48°. A bright vertical line can be observed in all of the pictures, which shifts from the right to the left side of the reflected beam spot as the incident angle increases. This vertical line is actually an indication of the Bragg-like retro-diffraction process. Similar effects have been observed on DFB laser devices [21]. The perfect resonance or the most efficient operation of the device corresponds to the overlap of the vertical light with the reflected laser beam spot. As shown in Fig. 4, the most efficient resonance mode is located at an incident angle of 35.7° for the TE-polarised laser beam at 532 nm, however, it is located at 30.2° for TM polarisation. These observations agree well with the spectroscopic response in Figs. 3*b* and *d*.

Furthermore, Fig. 3 also demonstrates high contrast and narrow bandwidth of the spectroscopic response of such a transparent waveguide grating structures. High contrast of the resonance signal can be identified by optical extinction spectrum with an amplitude as large as 0.34 OD and a nearly zero baseline on either side, e.g. as shown by the black spectrum in Fig. 3*b*, corresponding to an angle of incidence of 34°. The bandwidth of the optical extinction spectra shown in Fig. 3 can be as narrow as 6 nm at FWHM. However, in our previous research on waveguide grating structures, the resonance spectrum generally has an amplitude <0.2 OD and a bandwidth >10 nm. In particular, there can be observed a strong background that is asymmetric on both sides about the resonance spectrum [22–25].

Fig. 5 shows more detailed characterisation of the incident-angle-sensitive beam-splitting effects of the waveguide-grating device for a green laser beam at 532 nm. A total laser power was ∼102 mW at the incidence. Then, transmitted and reflected powers were measured at different angles of incidence. Transmittance (T) and reflectance (R) were calculated by $T = I_T/I_0$ and $R = I_R/I_0$, respectively, where I_T is the measured power of the transmitted laser beam, I_R is the reflected laser powers, the I_0 is the total laser power at the incidence.

Figs. 5*a* and *b* show the laser beam splitting performance at 532 nm for TE and TM polarisation, respectively, where the

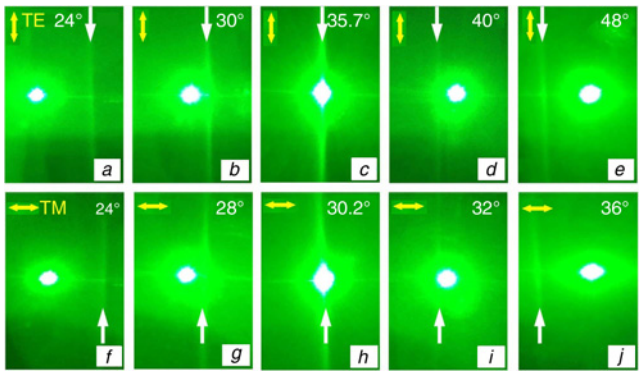

Fig. 4 *Photographs of the reflected laser beam spots at 532 nm at different angles of incidence, showing tuning of the Bragg-like retro-diffraction resonance mode for*
a–e TE and
f–i TM polarisation with the incident angle increased from 24° to 48°

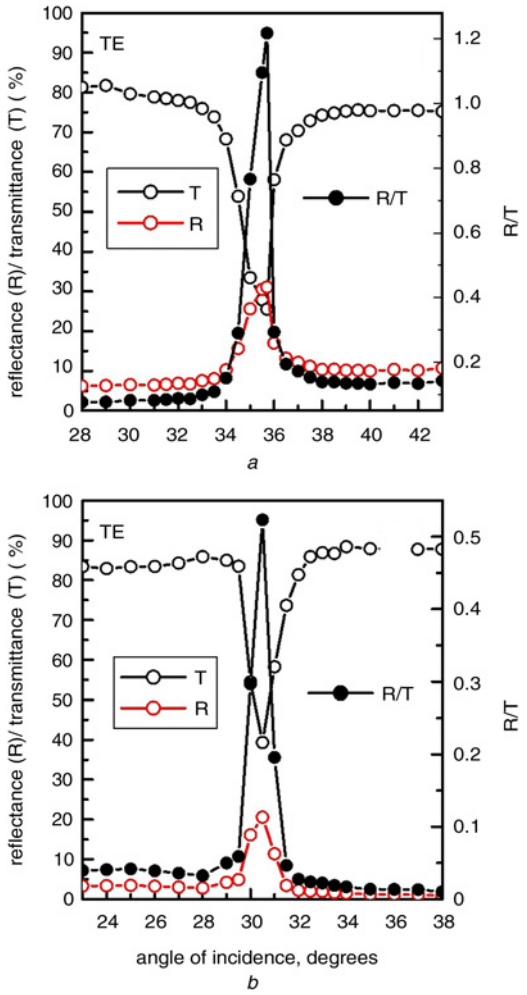

Fig. 5 *T and R versus incident angle for*
a TE and
b TM polarisation

incident angle was increased from 28 to 43° in Fig. 5*a* and from 23 to 38° in Fig. 5*b*. The resonance mode exhibits high sensitivity to the change in the incident angle, where the angle-resolved tuning curves in both Figs. 5*a* and *b* have a bandwidth of ~1.5° at FWHM. As shown in Fig. 5*a*, the transmission rate (T, black open circles) was changed from ~80% to ~26% and the reflection rate (R, red open circles) from ~0 to 31% for TE polarisation, when the incident angle was tuned from the perfect matching angle of 35.7°. The beam splitting ratio defined by R/T is plotted by the solid circles as a function of the incident angle in Fig. 5*a*, which is adjustable from 0 to 1.2 for TE polarisation. A splitting ratio of $R{:}T = 1{:}1$ was achieved at an angle of incidence between 35° and 36°, according to the curve of R/T by solid circles in Fig. 5*a*. In Fig. 5*b*, the transmission (T, black open circles) of the TM resonance mode was tuned from 88 to ~40% and the corresponding reflection (R, red open circles) was changed from ~0 to 21%. Thus, the beam splitting ratio (R/T, the solid circles) was changed from ~0 to 0.52. The narrow band width of the R/T curve in Fig. 5, which is <1° at FWHM, also indicates high incident-angle sensitivity of the beam splitting performance.

5.2. Beam splitting in different colours: Although the most efficient resonance mode was observed at ~530 nm, the narrow-band resonance may also take place in the blue and red spectral ranges according to Fig. 3. Fig. 6 shows the reflected beam spots in different colours, where the incident angle has been optimised so that the retro-diffraction is overlapped with the directly reflection

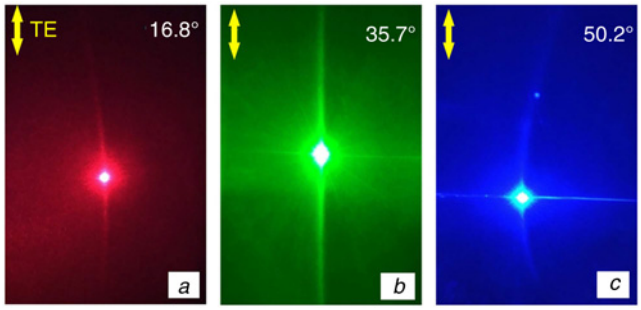

Fig. 6 *Photographs of the reflected laser beam spots at*
a 633 nm
b 532 nm and
c 470 nm, showing the patterns of resonance modes in different colours

to achieve the most efficient resonance for a specific wavelength. The pictures in Figs. 6*a–c* were taken for the red laser at 633 nm, the green laser at 532 nm, and the blue laser at 470 nm, respectively, for TE polarisation. These most efficient resonance modes were measured at different angles of incidence for different colours of lasers, which was at 16.8° for the red laser at 633 nm, at 35.7° for the green laser at 532 nm, and at 50.2° for the blue laser at 470 nm.

The most notable feature in Fig. 6 is that the vertical lines are arcing differently in different colours. A straight vertical line is observed for the green laser beam, however, the vertical line is curved to the left for the red and to the right for the blue laser beam. This implies that the most efficient resonance mode also corresponds to an optimised matching at a specific wavelength between the retro-diffraction and reflection patterns.

6. Conclusions: We demonstrated a single-layer thin-film optical beam splitter and summarise our advances in this research as follows: (i) A new photophysical process was revealed with the waveguide grating structures under the designed structural parameters, where a retro-diffraction process is overlapped with the normal waveguide-grating mode. The overlapped mode is equivalent to a second-order Bragg diffraction and is defined as the resonance mode of this transparent device, which is the basis for the high-efficiency and high-contrast beam-splitting performance. (ii) A simple and stable beam-splitting device consisting of a single ITO layer on a glass substrate was achieved, which operates efficiently within a narrow spectrum and is tunable in the visible band based on the sensitivity to the angle of incidence. This not only implies advantages over the conventional beam splitters, but also extends the functions of waveguide grating structures. (iii) The revealed mechanisms in this research also supplies applicable photophysics for the design of DFB lasers, tunable narrowband optical filters or polarisers, angle sensors, and optical switching devices.

7. Acknowledgments: This work was supported by the Program 973 (grant no. 2013CB922404), the National Natural Science Foundation of China (grant nos. 11574015 and 11434016) for the support.

8 References

[1] Rosenblatt D., Sharon A., Friesem A.A.: 'Resonant grating waveguide structures', *IEEE J. Quantum Electron.*, 1997, **33**, (11), pp. 2038–2059
[2] Christ A., Tikhodeev S.G., Gippius N.A., *ET AL.*: 'Waveguide-plasmon polaritons: strong coupling of photonic and electronic resonances in a metallic photonic crystal slab', *Phys. Rev. Lett.*, 2003, **91**, p. 183901

doi: 10.1049/mnl.2017.0082

[3] Feng S.F., Zhang X.P., Song J.Y., *ET AL.*: 'Theoretical analysis on the tuning dynamics of the waveguide–grating structures', *Opt. Express*, 2009, **17**, (2), pp. 426–436
[4] Fang Y., Tan Q.F., Zhang M.Q., *ET AL.*: 'Color separation of high-density dielectric rectangular grating in the Fresnel diffraction region', *Appl. Opt.*, 2012, **51**, (12), pp. 2172–2177
[5] Jing X.F., Zhang J.C., Jin S.Z., *ET AL.*: 'Design of highly efficient transmission gratings with deep etched triangular grooves', *Appl. Opt.*, 2012, **51**, (33), pp. 7920–7933
[6] Popov E., Wenger J., Hoose J., *ET AL.*: 'Strong three-dimensional field localization and enhancement on deep sinusoidal gratings with two-dimensional periodicity', *Opt. Lett.*, 2013, **38**, (22), pp. 4876–4879
[7] Sharon A., Rosenblatt D., Friesem A.A.: 'Narrow spectral band-widths with grating waveguide structures', *Appl. Phys. Lett.*, 1996, **69**, (27), pp. 4154–4156
[8] Xu T., Wu Y.K., Luo X.G., *ET AL.*: 'Plasmonic nanoresonators for high-resolution colour filtering and spectral imaging', *Nat. Commun.*, 2010, **1**, p. 59.
[9] Zhang X.P., Liu H.M., Tian J.R., *ET AL.*: 'Band-selective optical polarizer based on gold-nanowire plasmonic diffraction gratings', *Nano Lett.*., 2008, **8**, (9), pp. 2653–2658
[10] Yu Z.N., Deshpande P., Wu W., *ET AL.*: 'Reflective polarizer based on a stacked double-layer subwavelength metal grating structure fabricated using nanoimprint lithography', *Appl. Phys. Lett.*, 2000, **77**, (7), pp. 927–929
[11] Zhang X.P., Ma X.M., Dou F., *ET AL.*: 'A biosensor based on metallic photonic crystals for the detection of specific bioreactions', *Adv. Funct. Mater.*, 2011, **21**, (22), pp. 4219–4227
[12] Nau D., Seidel A., Orzekowsky R.B., *ET AL.*: 'Hydrogen sensor based on metallic photonic crystal slabs', *Opt. Lett.*, 2010, **35**, (18), pp. 3150–3152
[13] Zhang X.P., Sun B.Q., Hodgkiss J.M., *ET AL.*: 'Tunable ultrafast optical switching via waveguided gold nanowires', *Adv. Mater.*, 2008, **20**, (23), pp. 4455–4459
[14] Mateus C.F.R., M. Huang C.Y., Chen L., *ET AL.*: 'Broad-band mirror (1.12–1.62 μm) using a subwavelength grating', *IEEE Photon. Technol. Lett.*, 2004, **16**, (7), pp. 1676–1678
[15] Zheng J., Ye Z.C., Sun N.L., *ET AL.*: 'Highly anisotropic metasurface: a polarized beam splitter and hologram', *Sci. Rep.*, 2014, **4**, p. 6491
[16] Zhai T.R., Zhang X.P.: 'Gain- and feedback-channel matching in lasers based on radiative-waveguide gratings', *Appl. Phys. Lett.*, 2012, **101**, (14), p. 143507
[17] Saliba M., Wood S.M., Patel J.B., *ET AL.*: 'Structured organic–inorganic perovskite toward a distributed feedback laser', *Adv. Mater.*, 2016, **28**, (5), pp. 923–929
[18] Hao L.J., Shi Y.C., Xiao R.L., *ET AL.*: 'Study on sampled waveguide grating with antisymmetric periodic structure', *Opt. Express*, 2015, **23**, (12), pp. 15784–15791
[19] Halir R., Bock P.J., Cheben P., *ET AL.*: 'Waveguide sub-wavelength structures: a review of principles and applications', *Laser Photon. Rev.*, 2015, **9**, (1), pp. 25–49
[20] Jia P.P., Yang J.: 'A plasmonic optical fiber patterned by template transfer as a high-performance flexible nanoprobe for real-time biosensing', *Nanoscale*, 2014, **6**, (15), pp. 8836–8843
[21] Zhai T.R., Zhang X.P., Pang Z.G., *ET AL.*: 'Direct writing of polymer lasers using interference ablation', *Adv. Mater.*, 2011, **23**, (16), pp. 1860–1864
[22] Li R., Zhang X.P., Kong L.: 'Single-shot fabrication of waveguide ternary gratings with narrow-band optical response', *J. Nanosci. Nanotechnol.*, 2011, **11**, pp. 1047–1051
[23] Feng S.F., Zhang X.P., Liu H.M.: 'Fiber coupled waveguide grating structures', *Appl. Phys. Lett.*, 2010, **96**, p. 133101
[24] He J.F., Zhang X.P.: 'Fiber-based flexible interference lithography for photonic nanopatterning', *Opt. Express*, 2014, **22**, pp. 26386–26391
[25] Zhang X.P., Feng S.F., Zhai T.R.: 'Energy transfer channels at the diffraction-anomaly in transparent gratings and applications in sensors', *Photonics Nanostruct. Fundam. Appl.*, 2013, **11**, pp. 109–114